Journal of Pharmaceutical Sciences 111 (2022) 368–381

Contents lists available at ScienceDirect

Journal of Pharmaceutical Sciences

journal homepage: www.jpharmsci.org

Pharmaceutical Biotechnology

Understanding Heat Transfer During the Secondary Drying Stage of Freeze Drying: Current Practice and Knowledge Gaps

Kyu Yoon, Vivek Narsimhan*

Davidson School of Chemical Engineering, Purdue University, West Lafayette, IN 47907, USA

ARTICLE INFO

Article history:
Received 30 May 2021
Revised 20 September 2021
Accepted 21 September 2021
Available online 24 September 2021

Keywords:
Secondary drying
Lyophilization
Freeze-drying
Heat and mass transfer
Mathematical model

ABSTRACT

Currently, there is a lack of robust models for secondary drying with comparable accuracy and flexibility as primary drying models. In order to better understand heat transfer during secondary drying, sucrose and mannitol solutions were freeze-dried in vials in a lab-scale lyophilizer under various drying conditions. Several distinct thermal characteristics for secondary drying were experimentally observed: (1) the vial heat transfer coefficient can change significantly between primary and secondary drying due to the change in water vapor content in the freeze dryer; (2) the thermal mass of the vial plays a major role in determining the cake temperature as roughly 95% of the heat supplied is absorbed by the vial walls. From a theoretical perspective, three different models of secondary drying were examined with varying degrees of complexity (full 3D simulation, 1D-averaged equations, and lumped-capacitance 0D approach). In these models, the desorption of bound water is treated as a one-way coupling with temperature. It is found that although a simple lumped-capacitance approach can capture many of the vital features of cake temperature and moisture profile, near quantitative agreement with experiments can be made by employing a 1D-averaged equation approach, where the effective thermal conductivities of the vial are determined by thermal circuits.

Nomenclature

A	Surface area of the material [mm^2]
A_{ck}	Cross-sectional area occupied by cake [mm^2]
A_{tot}	Surface area of the heat flux sensor [mm^2]
A_v	Surface area of the bottom of the vial [mm^2]
A_{wall}	Cross-sectional area of the glass wall (in the z-direction).
Bi	Biot number [-]
c_w	Moisture content at the cake [kg water/kg cake]
c_w^*	Equilibrium moisture content [kg water/kg cake]
C_P	Heat capacity [kJ/kg/K]
C_1	Thermal mass per unit volume in the first region ($0 \le z \le L_b + L_{ck}$) [kJ/m^3]
C_2	Thermal mass per unit volume in the second region ($L_b + L_{ck} \le z \le L_v$) [kJ/m^3]
E_a	Activation energy [kJ/mol]
k	Thermal conductivity [W/m/K]
k_{eff}	Effective thermal conductivity [W/m/K]
k_g	Rate constant of the desorption kinetic [1/s]
$k_{g,0}$	Rate constant at reference temperature T^{ref} [1/s]
K_{tot}	Heat transfer coefficient at the heat flux sensor [W/m^2/K]
K_{air}	Heat transfer coefficient of the air at the heat flux sensor [W/m^2/K]
K_{top}	Heat transfer coefficient at the top of the vial [W/m^2/K]
K_v	Heat transfer coefficient at the bottom of the vial [W/m^2/K]
K_v^{pri}	Vial heat transfer coefficient during primary drying [W/m^2/K]
K_v^{sec}	Vial heat transfer coefficient during secondary drying [W/m^2/K]
L_b	Bottom thickness of the vial [mm]
L_{ck}	Length of the cake [mm]
L_v	Length of vial [mm]
$\dot{m}_{sub}$	the mass per unit time of water vapor sublimated [g/h]
m_1	Fitting parameter for equilibrium moisture content (Eq. 4) [(kg water/kg cake)$^{0.5}$/K]
m_2	Fitting parameter for equilibrium moisture content (Eq. 4) [(kg water/kg cake)$^{0.5}$]
n	Normal vector [-]
N	Number of the elements used in the simulation [-]
p_{ch}	Chamber pressure [mTorr]
q	Heat flux [W/m^2]
q_{sub}	Sublimation heat flux [W/m^2]
Q_T	Total heat flow [W]
r	r-component (radial direction) [mm]

* Corresponding author.
E-mail address: vnarsim@purdue.edu (V. Narsimhan).

https://doi.org/10.1016/j.xphs.2021.09.032
0022-3549/

R_g	Natural gas law constant [J/mol/K]
R^2	Standard error [-]
t	Time [s]
T	Temperature [°C]
T_p	Temperature of the product (ice or cake) [°C]
T_{ref}	Reference temperature for desorption kinetics [K]
T_{sh}	Shelf temperature [°C]
T_{sim}	Temperature of the lyosim [°C]
T_{top}	Temperature at the top boundary of the vial [°C]
V	Volume [mm^3]
V_v	Volume of the vial [mm^3]
z	z-component (vertical direction) [mm]

Greek letter

α	Index of the materials [-]
γ	Index of the materials [-]
Δc_w	Change in moisture content of the cake [kg water/kg solid]
ΔH_{sub}	Enthalphy of sublimation [kJ/kg]
ΔH_v	Latent heat of water desorption [kJ/kg]
Δt	Time interval during drying process [h]
Δt_s	Time step [min]
$<\Delta T>$	Average temperature difference between shelf and product during time interval [°C]
Δx	Mesh size of the intermediate fidelity model [mm]
ρ	Density [kg/m3]

Subscript

air	Air
ck	Cake
glass	Glass
ice	Ice
1	First region ($0 \leq z \leq L_b + L_{ck}$) for the intermediate fidelity model
2	Second region ($L_b + L_{ck} \leq z \leq L_v$) for the intermediate fidelity model

Introduction

Freeze-drying or lyophilization is widely used for the long-term preservation of biological materials and pharmaceuticals such as proteins, vaccines, antineoplastics, peptide hormones, and high-quality foods.[1,2] This process has been broadly adopted because lyophilization is an effective way of drying materials without harming their quality including biological, nutritional, and organoleptic properties. During lyophilization, the product is dried by freezing the material and promoting the direct transition of the solvent (typically water) from a solid phase to the gas phase without passing through the liquid phase.[3] Because this process avoids high temperatures, it is found that chemical decomposition or denaturation is minimized, especially when the heat sensitive material is dissolved in the solution. In addition, the lyophilized product can be quickly reconstituted with water because the product has an interconnected porous structure with a high specific surface area.[4,5]

However, one disadvantage of lyophilization is that it is an energy- and time-consuming process. Many biological products such as proteins, liposomes, and vaccines can also be damaged by freeze-drying if one does not consider the thermal properties of these materials. In addition, the manufacturing cost of final product directly depends on optimization and selection of design space in the lyophilization process.[6,7] In current practice in lyophilization, the setpoint values are chosen conservatively which leads to an energy efficiency of less than 5% for the cycle.[7] The entire freeze-drying process could take days or even weeks to finish when these input conditions are not optimized.[2,8] From these reasons, it is currently limited to high-added-value products.

To overcome these limitations, a lot of research was devoted to the optimization of lyophilization based on mathematical modeling. Lyophilization consists of three steps – freezing, primary drying (i.e., sublimation of ice), and secondary drying (i.e., removal of bound water). Of the three steps, primary drying is relatively well understood since this process is usually the longest part of the cycle[9] and its optimization reduces the operation time resulting in a faster throughput for a given freeze dryer.[6] Existing research has explored how operating conditions and material properties of the excipient affect the drying time and cake temperature.[10–13] Pikal and coworkers in particular studied how to identify the end point of the primary drying process.[14–16] Two-dimensional theoretical models were developed to get information not easy to obtain from experiments and to suggest the design of a freeze-drying process.[17–24] In these models, heat and mass transfer equations were solved in the frozen and dried regions of the cake along with boundary conditions at the sublimation front. Shivkumar et al. (2019) proposed a simple lyophilization calculator for the freezing and primary drying steps, to be used as a primary drying design-space generator and as a process optimizer.[7]

The last step of freeze-drying – the secondary drying stage – is also important in improving drying efficiency because this process takes ~10–20% of the total drying time and 12–20% of the operational cost.[25] In this stage, the porous cake is heated for more than 3 –25 h to remove any bound water remaining in the sample and get the final moisture to a desired range of 1 wt% or below.[26] Therefore, special attention has been paid to the development and optimization of the final drying step as well in the production technology for lyophilization.

Several studies have contributed to understanding the rate-limiting mechanisms of water desorption .[18,27,28] Impacts on the secondary drying kinetics were described as a function of temperature, chamber pressure, and partial pressure of water vapor.[27,29] Real-time measurements of chamber pressure, mass flux, mass balance, and heat flux were adopted to monitor the desorption kinetics and understand the drying process.[30–36] These measurements of desorption kinetics are coupled with a desorption model and fitted parameters to match the rate of mass change over time. Based on the amount of residual water at the end of the primary drying process, the evolution of moisture content in the product during secondary drying and the drying time required to achieve the target moisture content can be estimated.

Meanwhile, modeling of secondary drying has been improved based on experimental approaches in the recent decade. Experiment-based models were empirically optimized using many experiments with a variety of temperature regimes and changes of other parameters.[33,37–39] In modeling, it is generally assumed that the domain of interest and the heat transfer parameters will be the same as those in the primary drying process. We will show in this paper that these assumptions may become invalid and could be a reason why there is a lack of robust models for secondary drying with comparable accuracy and flexibility as primary drying models. Studies clarifying the uncertainties in the secondary drying process will be vital to quantitative understanding and optimization of secondary drying in lyophilizers.

Outline

In this paper, we perform a set of detailed experiments to gain a better understanding of the heat transfer during secondary drying for pharmaceutical applications. These experiments are accompanied by several mathematical models of various degrees of complexity, in order to access which approaches are most viable for a practical and accurate representation of temperature profile and moisture content. The aim in this paper is to illuminate the several important

observations that will be helpful for future investigations of secondary drying. The main findings observed are:

1. The thermal mass of the container such as vial, syringe, and drug-device cartridge plays an outsized role in determining the temperature of the cake during secondary drying. If one performs a simple order-of-magnitude analysis for a glass vial, one sees that the vial walls absorb up to 95% of the heat supplied during secondary drying. Thus, the thermal properties of the cake (e.g., heat capacity and thermal conductivity) and the latent heat from bound water desorption do not appreciably affect the cake's temperature profile for the typical fill volumes used in pharmaceutical applications (~2 mL).
2. The heat transfer coefficient from the shelf to the vial is significantly different (~50% lower) during secondary drying than the values reported in the literature for primary drying, possibly due to the change in water vapor content in the freeze dryer. These updated heat transfer coefficients are necessary in order to model the heat transfer quantitatively without fitting parameters.
3. From a modeling standpoint, the temperature and moisture content in the cake can be described via one-way coupling, where the moisture content does not alter the cake's temperature profile. A simple, 0D lumped-capacitance approach can capture many of the trends for the temperature profile over time, but the temperature is over-estimated compared to experiments. One can obtain near quantitative agreement with experiments by employing a 1D-averaged equation approach, where the effective thermal conductivities of the lumped vial plus cake are determined by a thermal circuit analysis.

We hope that this paper will help eliminate some of the uncertainties associated with heat transfer modeling for secondary drying. In Section 3, we describe the freeze-drying setup as well as the excipients and drying conditions studied. In Section 4, we perform an order-of-magnitude analysis to determine the major factors governing heat transfer in secondary drying, and obtain experimental measurements of heat transfer coefficients. Section 5 goes over the three mathematical models developed, and Section 6 compares the models to experimental measurements of cake temperature and moisture content. Conclusions follow in Section 7.

Materials and Methods

Materials

In this study, 5 wt% sugar is dissolved in deionized water. Here, we select sucrose (Sigma-Aldrich, St. Louis, MO) and mannitol (Pfanstiehl Inc., Waukegan, IL) as excipients. The vials used for lyophilization are Fiolax Clear 6R Vials (SCHOTT, Mullheim, Germany) with 3D printed lyophilization stoppers.

Freeze-Drying

We use the laboratory-scale freeze-dryer MicroFD (Millrock Technology, Kingston, NY) for our experiments as schematically described in Fig. 1. The shelf of the freeze-dryer is fully loaded with nineteen 6R vials, and each vial is filled with 2 mL of 5 wt% excipient (sucrose or mannitol) solution. It is common to use a low coefficient of fullness for pharmaceuticals in order to achieve a reasonable drying time, and a fill volume of 2 mL in a 6R vial is a standard choice.[7,22,40]

During the steps of freezing, primary drying, and secondary drying, we control the shelf temperature (T_{sh}) and the chamber pressure (p_{ch}) of the freeze-dryer. We record the product temperature (T_p) in the central vial using a specially-made probe placed at the center of the sugar solution/cake. We also record the energy transferred to the vials using a heat flux sensor located underneath the vials. The idea of using heat flux sensors to track energy flow during freeze drying is a relatively new technology in the pharmaceutical space – an excellent discussion of this technology is in .[36,41] Lastly, to ensure homogeneity in heating all the vials in the chamber, we control the

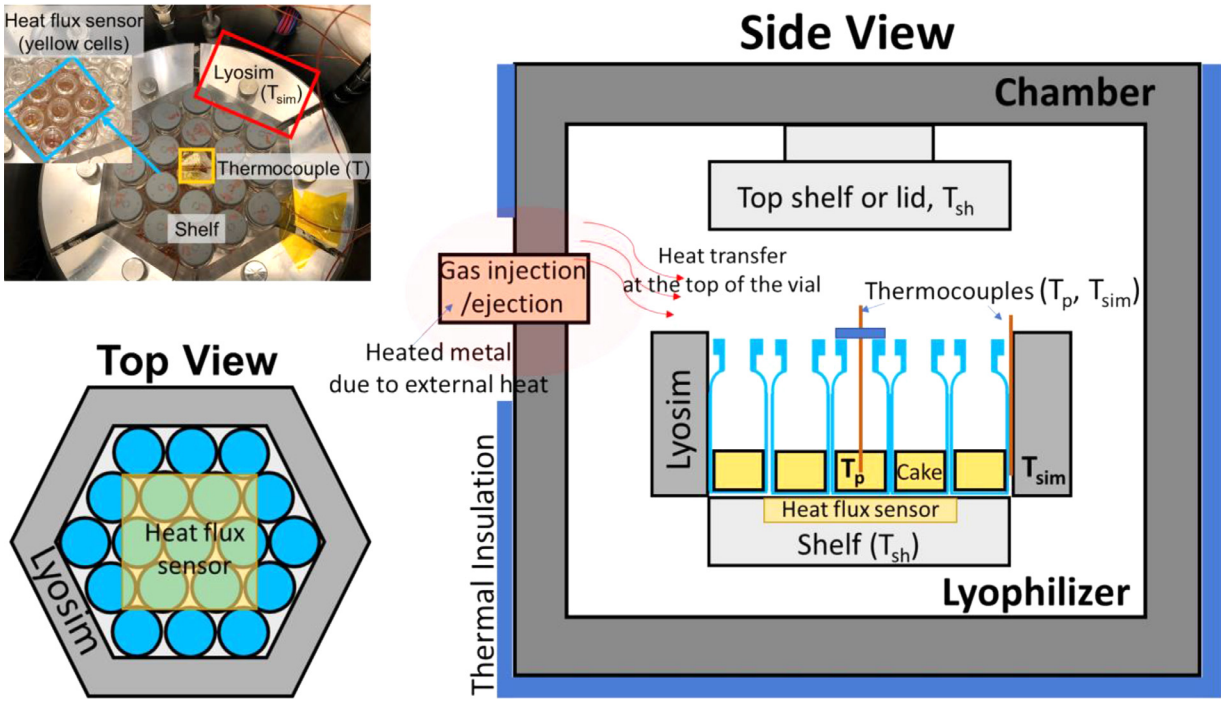

Fig. 1. Schematic diagram of the freeze dryer system.

temperature of the outer aluminum blocks that make direct contact with the outer vials (T_{sim}, see Fig. 1). We set the temperature of the outer blocks equal to that of the measured product temperature ($T_{sim} = T_p$). The details on how we perform this temperature matching procedure are mentioned in the supporting information. Figs. S1 and S2 in the supporting information show that the measured temperature difference between the aluminum block and the product temperature is small, and hence the heat transfer from the shelf to each vial is uniformly distributed in the lyophilizer under this experimental setup.

The shelf temperatures and chamber pressures during freeze-drying are as follows. For freezing, we ramp the shelf temperature T_{sh} from room temperature to −40°C at a rate of −1°C/min and hold the temperature for 1 hour at -40°C at a chamber pressure of $p_{ch} =$ 110 mTorr. After freezing, primary drying is carried out by ramping the temperature to $T_{sh} =$−20°C at a rate of 1°C/min, and then maintaining the temperature at T_{sh} = -20°C for 30 hours with the chamber pressure at $p_{ch} =$ 100 mTorr. To verify that primary drying has completed, we measure the pressure using a Pirani gauge and a capacitance manometer (CM), and use the well-known fact that the difference between these two measurements indicate the presence of water vapor and hence sublimation.[15] During secondary drying, the shelf temperature is ramped from $T_{sh} =$ −20°C to a final temperature T_{sh} = 15 to 35°C at a rate of 1°C/min, and the final temperature is held for 6 hours at a chamber pressure 100 mTorr. After secondary drying, the moisture content of the sample is determined (see Section 3.3).

One special note that we would like to make is that during our measurements, the cake temperature measured during freeze drying will not necessarily match the shelf temperature at steady-state since the temperature in the freeze-dryer's air chamber is different than the shelf temperature due to energy transfer from a pressure control valve (at T_{top} ~30°C) and small amounts of air being injected from the outside to control the chamber pressure. This effect is negligible in large-scale freeze dryers, but is important for smaller scale freeze dryers. It will result in heat transfer to the top of the vial, which will be estimated as a heat transfer coefficient. More details are in Section 4.3.

Equilibrium Moisture Content

Residual moisture quantification was carried out with the Computrac Vapor Pro® XL (AMETEK BrookField, Middleborough, MA) as an alternative to Karl Fischer titration method.[42] The device heats up the injected vial and the moisture is driven off and measured by a calibrated relative humidity sensor. Five vials per each case were randomly selected after end of the secondary drying process to measure the equilibrium moisture content of the cake. Fig. S3 in the supporting information shows that the moisture content during secondary drying does not depend on vial's location in the chamber, indicating that the chamber's heating is homogenous.

Experimental Results

Observations and Order-of-Magnitude Analysis

Fig. 2a shows a typical temperature profile versus time for 5% wt sucrose during primary and secondary drying. The vertical, dotted line signifies the end of primary drying, which occurs when the Pirani gauge pressure matches the capacitance manometer pressure (Fig. 2b). At this point, the measured moisture content of the cake is 4.1% water by mass. Using this experimental information and the reported thermal properties of the vial, air, frozen solution (ice), and cake (Table 1), we can provide an order-of-magnitude estimate for how much energy is consumed by various processes during primary and secondary drying (Table 2). Overall, Table 2 shows that the majority of energy supplied during primary drying is used to sublimate the ice. However, this picture looks quite different during secondary drying. In secondary drying, ~95% of the supplied energy heats the glass walls of the vial rather than heating the cake or desorbing bound water. One will obtain similar estimates if one examines other data in the literature with similar fill volumes.[7,43]

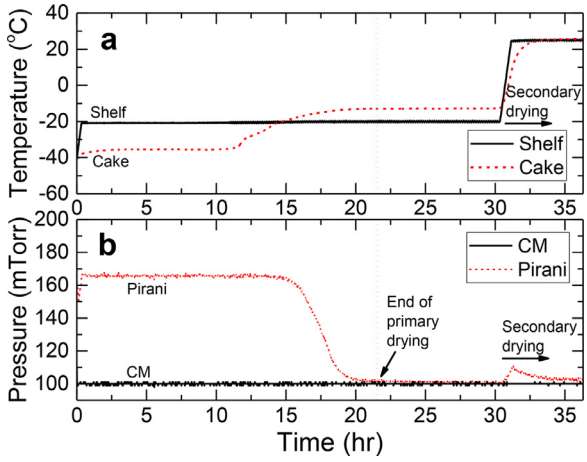

Fig. 2. Typical (a) temperature and (b) pressure profiles versus time for 5% wt sucrose during primary and secondary drying. The vertical, dotted line signifies the end of primary drying, which occurs when the Pirani gauge pressure matches the capacitance manometer pressure.

What this analysis indicates is that secondary drying is an incredibly inefficient process, since a small fraction of the supplied heat is actually used to desorb water. It also indicates that the thermal mass of the vial plays an outsized role in determining the temperature profile of the cake, and that the thermal properties of the cake and the desorption of bound water have a minimal effect on the cake's temperature. Fig. 3 shows the temperature profile for mannitol and sucrose during secondary drying at different shelf temperatures ($15^oC \leq T_{sh} \leq 35^oC$). The temperature profiles of the two excipients are indistinguishable even though they have different thermal properties and that the sucrose cake shrinks and partially loses contact with the glass wall.[44,45] This is strong evidence that the cake's thermal properties play a minor role in the overall heat transfer.

Another point that this analysis suggests is that the heat transfer coefficient between the shelf and vial bottom may exhibit significant differences during primary and secondary drying. If we use the data from Fig. 2 that primary drying takes $\Delta t \approx$ 10 hours and secondary drying takes $\Delta t \approx$ 2.5 hours, the heat transferred per unit time per unit area to the vial bottom is roughly $K_v \approx \frac{Q_T}{\langle T_{sh}-T_p \rangle} A_v \approx 16.0\ W/(m^2 * K)$ for primary drying, and $K_v \approx \frac{Q_T}{\langle T_{sh}-T_p \rangle} A_v \approx 9.8\ W/(m^2 * K)$ for secondary drying, where $A_v = 3.80 * 10^{-4}\ m^2$ is the area of the vial bottom and $T_{sh} - T_p$ is the average difference between the shelf and product temperature during the time period. These expressions assume that the product temperature is similar to the temperature at the bottom of the vial (i.e., $T_p \approx T_v$). The next subsection (Section 4.2) will discuss this point in more detail and provide precise experimental measurements of the heat transfer coefficients.

Measurement of Heat Transfer Coefficients at Bottom of Vial

Comment on Different Types of Heat Transfer Coefficients

The heat transfer coefficient between the shelf and the vial bottom is equal to the heat flux applied to the vial divided by the temperature difference between the shelf and vial bottom: $K_v = q_{vial}/(T_{sh} - T_v)$. In this manuscript, the temperature probe is not located at the vial bottom but rather in the middle of the product.

Table 1
Material properties and model parameters used in theoretical models.

Parameter	Materials				
	Vial (Glass)	Air	Frozen solution	Cake (Sucrose)	Cake (Mannitol)
ρ [kg/m3]	2.20×10^3	1.57×10^{-4}	918	91.2	44.2
C_P [kJ/kg/K]	0.84	1.00	2.05	1.00	1.72[a]
k [W/m/K]	1.20	0.026	2.22	0.0282[b]	0.0277[c]
A [mm^2]	3.80×10^2		3.14×10^2	2.16×10^2	3.14×10^2
L [mm]			7.0	4.9	7.0
V [mm^3]	3490.3	8704.4	2152.3	1017.6	2152.3
E_a [kJ/mol]				8.31[a]	13.42[d]
$k_{g,0}$ [1/s]				2.0×10^{-4}	2.0×10^{-4}
ΔH_{sub} [kJ/kg]			2834.6*		
ΔH_v [kJ/kg]				2499.6[a]	2840.2[b]

[a] Pikal et al. (2005)[22]
[b] Ravnik et al. (2018)[40]
[c] Mascarenhas et al. (1997)[20]
[d] Oddone et al. (2017)[35]

Table 2
Order-of-magnitude estimate for how much energy is consumed by various processes during primary and secondary drying from experimental observations of 2 mL of 5 wt% sucrose (see Fig. 2a). Time intervals used for the analysis are 0 < t < 10 hr for primary drying and 0.5 < t < 3 hr for secondary drying, respectively. Parameters used in energy budget analysis are listed in Table 1. It is assumed that the initial and final moisture content of the cake are 4.08 wt% and 1.48 wt% during the time interval of secondary drying based on Eq. 2 in Section 4.4 using the experimental temperature profile. The temperature change (ΔT) during primary drying and secondary drying is 5.0°C and 29.2°C, respectively. It is also assumed that the temperature of the ice (or cake) has the same temperature as the surroundings (vial or air).

Category of the energy consumption	Energy [J]	
	Primary drying (0 h < t <10 h)	Secondary drying (0.5 h < t < 3 h)
Glass vial: $\rho_{glass}\ C_{p,glass}\ V_v \Delta T_{glass}$	32.5	1.90×10^2 (95%)
Ice: $\rho_{ice} C_{p,ice}\ V_{ice}\ \Delta T_{ice}$	41.9	N/A
Cake: $\rho_{ck} C_{p,ck}\ V_{ck} \Delta T_{ck}$	N/A	2.70
Air: $\rho_{air} C_{p,air}\ V_{air}\ \Delta T_{air}$	5.58×10^{-4}	3.69×10^{-2}
Sublimation of ice: $m_{sub}\ \Delta H_{sub}$	3.15×10^3 (98%)	N/A
Water desorption: $\Delta c_w \rho_{ck} V_{ck} \Delta H_v$	N/A	6.49
Total: Q_T	3.22×10^3	1.99×10^2

Thus, this paper measures the effective heat transfer coefficient between the shelf and the product: $K_v^{eff} = q_{vial}/(T_{sh} - T_p)$. The two heat transfer coefficients can be considered equal when there is negligible temperature difference between the vial and the product (i.e., $|T_p - T_v| \ll |T_v - T_{sh}|$) – in other words, the Biot number based on the product half-thickness is negligible: $Bi_{prod} = R_{prod}/R_{shelf} < 0.1$, where R_{prod} is the thermal resistance in the lower half of the product and R_{shelf} is the resistance from the shelf to the vial. In the supporting information, we show that the Biot number is less than 0.1 for the fill volumes used during primary and secondary drying, and that the measured temperature difference between the product and vial is less than 0.7°C during the freeze drying cycle except the case when T_p measures temperature at the cake but sublimation is still in progress (Figures S4-S5 in Supporting Info). Therefore, the heat transfer coefficient between shelf and product in this paper can be regarded as the vial heat transfer coefficient.

Experimental Measurements Via Heat Flux Sensor

This section performs measurements of the vial heat transfer coefficient K_v by placing temperature probes on the shelf and in the center of the cake, as well as a heat flux sensor underneath several vials as described in Fig. 1. Below lists the experimental procedure to determine K_v and the results for primary and secondary drying.

Fig. 4a shows the temperature profile over time for the shelf and cake during primary and secondary drying, and Fig. 4b shows the corresponding measurements of heat flux (q) versus temperature difference ($T_{sh} - T_p$) between the shelf and cake. The graphs are labelled by six distinct regions. Region 1 occurs during the ramping stage of primary drying (0 < t < 0.33 hr) where the shelf temperature increases from the freezing temperature $T_{sh} = -40^oC$ to the primary drying temperature $T_{sh} = -20^oC$. The second region occurs during the sublimation stage where the shelf temperature and cake temperatures are relatively constant. The third stage shows the transition from ice to cake at the observation point when sublimation front passes the thermocouple. The fourth stage is the end stage of

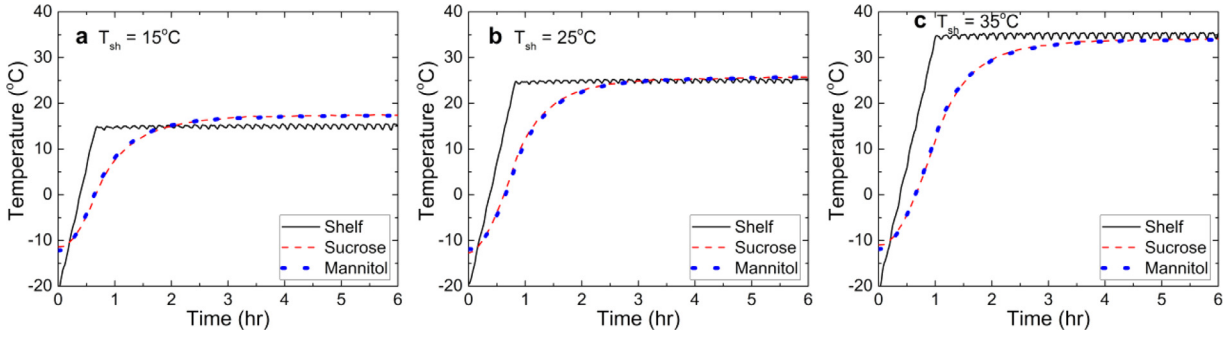

Fig. 3. Comparison of measured product temperature profiles during secondary drying of an aqueous solution containing 5 w/v% sucrose (red) and 5 w/v% mannitol (blue). The shelf temperature during secondary drying process is (a) 15°C, (b) 25°C, and (c) 35°C.

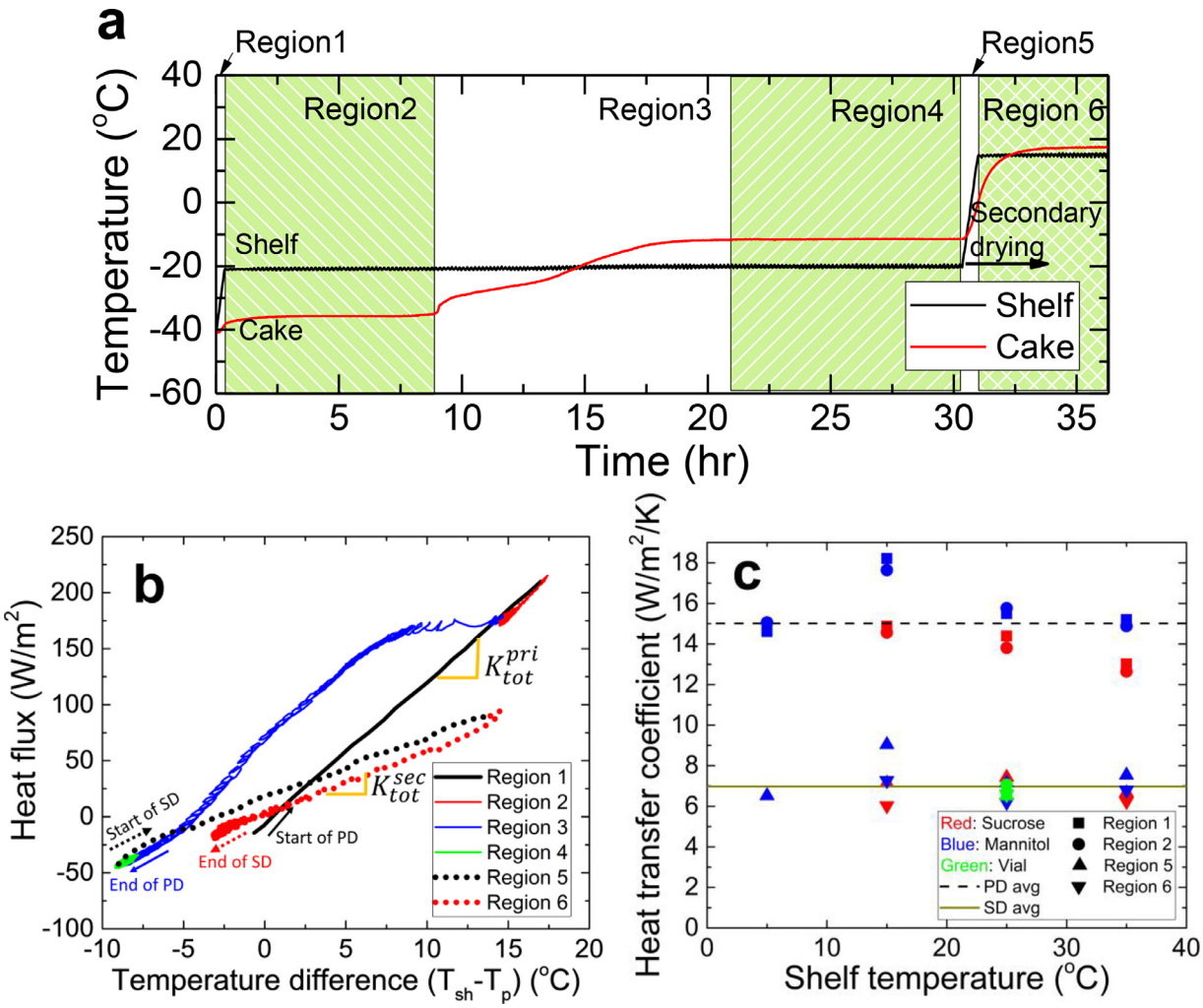

Fig. 4. (a) The temperature profile over time for the shelf and cake during primary and secondary drying with 6 distinct regions, (b) measurements of heat flux versus temperature difference ($T_{sh} - T_p$) between the shelf and cake during primary and secondary drying, and (c) the vial heat transfer coefficients measured during primary drying (region 1-2 in Fig. 4a-b) and secondary drying (regions 5-6 in Fig. 4a-b) for sucrose (red), mannitol (blue), and empty vial (green) and different final shelf temperatures at the end of secondary drying (T_{sh} = 5, 15, 25, and 35°C).

primary drying, where most sublimation has finished and the cake temperature increases. The fifth and sixth stages indicate secondary drying. The fifth stage is when the shelf temperature ramps up during secondary drying, while the sixth stage is when the shelf temperature is constant. Typically, primary drying heat transfer coefficients are measured during the first and second stage (0 < t < 10 h) where the heat flux versus temperature difference has a constant slope. We see that the heat transfer characteristics during secondary drying (stages 5–6) are considerably different from that during primary drying (stage 1–2).

To estimate the vial heat transfer coefficient K_v, we first define the overall heat transfer coefficient of the sensor K_{tot} as the ratio of the measured heat flux and the temperature difference from Fig. 4b: i.e., $K_{tot} = q/(T_{sh} - T_p)$. We note that this heat transfer coefficient contains contributions from the vial and the air since the sensor is partially occupied by hexagonal array of vials (7 vials in total). The overall heat transfer coefficient for single vial, K_v, is related to K_{tot} by $K_{tot}A_{tot} = N_v K_v A_v + K_{air}(A_{tot} - N_v A_v)$, where A_{tot} is the area of the sensor, A_v is the area occupied by the bottom of a single vial, N_v is the number of vials on the heat flux sensor based on hexagonal packing,[41] and K_{air} is the heat transfer coefficient to the air which was determined by a separate measurement without the vials in place. Further details of this process are found in the supporting information (Figs. S6 and S7).

Fig. 4c shows the vial heat transfer coefficients measured during primary drying (region 1–2 in Fig. 4a-b) and secondary drying (regions 5–6 in Fig. 4a-b) for different excipients (sucrose and mannitol) and different final shelf temperatures at the end of secondary drying (15°C ≤ T_{sh} ≤ 35°C). The measurements do not vary considerably depending on the shelf temperature and excipient. Furthermore, the values obtained are consistent with prior methods of measuring heat transfer coefficients in the literature. The vial heat transfer coefficient during primary drying is $K_v^{pri} = 15.01 \pm 3.20\ W/(m^2\ K)$ and it is comparable to measurements of $K_v^{pri} = 15.09 \pm 2.01$ W/(m^2 K) by Pikal (1985)[17] and $K_v^{pri} = 15.06$ W/(m^2 K) by Shivkumar et al. (2019)[7] within 0.5% error for a 6R vials at 100 mTorr chamber pressure. In those papers, a heat flux sensor was not available, and the heat transfer coefficient was instead estimated from a gravimetric analysis as $K_v^{pri} \approx q_{sub}\frac{1}{T_{sh}-T_v} = \frac{\dot{m}_{sub}\Delta H_{sub}}{A_v}\frac{1}{T_{sh}-T_v}$, where q_{sub} is the sublimation heat flux, $\dot{m}_{sub}$ is the mass per unit time of water vapor sublimated, ΔH_{sub} is the enthalpy per unit mass for sublimation, A_v is the area of the bottom vial, and $T_{sh} - T_v$ is the temperature difference between the shelf and the bottom of the vial.

The measured heat transfer coefficient for secondary drying is $K_v^{sec} = 6.97 \pm 2.07$ W/(m^2 K) for a 6R vial at 100 mTorr chamber pressure, which is a factor of ~2 smaller than the reported values during the initial stages of primary drying. A possible reason for

this observation is that water vapor is present during primary drying, which alters the conductivity of gas between the vial bottom and shelf and also alters the flow rate in the chamber due to sublimation. We note that if one performs a heat transfer coefficient measurement on empty vials in a dry chamber, one obtains the same value as in secondary drying (Fig. 4c). Additional measurements are shown in Fig. S8 in the supporting information. All this data seem to indicate that the vial heat transfer coefficient is different during secondary drying, at least for the small-scale equipment used in this study. It is noted that knowing this value is vital for accurate modeling of freeze-drying.

Measurement of Heat Transfer Coefficient at Top of Vial

As mentioned previously in Section 3.2, the temperature in the freeze-dryer's air chamber is different than the shelf temperature due to energy transfer from a valve (at $T_{top} \approx 30^oC$) and small amounts of air being injected from the outside to control the chamber pressure. This phenomenon results in additional heat transfer to the top of the vial, which is generally negligible for large-scale freeze dryers but must be considered for laboratory-scale freeze dryers for accurate heat transfer modeling. To determine the effective heat transfer coefficient K_{top} from this effect, we record the steady-state cake temperature T_p just before the start of secondary drying (i.e., end of region 4 in Fig. 4b) and at end of secondary drying (i.e., end of region 6 in Fig. 4b), and plot these temperatures as a function of the shelf temperature T_{sh} in Fig. 5. By performing a steady macroscopic energy balance on the vial, we determine K_{top} by solving:

$$K_{top}A_v\left(T_p - T_{top}\right) = K_v^{sec}A_v\left(T_{sh} - T_p\right) \quad (1)$$

where $K_v^{sec} = 6.97\ W/(m^2\ K)$ is the vial heat transfer coefficient for secondary drying. From Fig. 5, we see that the vial temperature is the same as the shelf temperature when $T = 30^oC$, which indicates that $T_{top} = 30^oC$. Performing the best fit on the data yields $K_{top} = 1.65$ W/(m^2 K). We will use this heat transfer coefficient in our modeling, although we note that the exact value of this coefficient doesn't change the qualitative conclusions discussed in this manuscript.

Equilibrium Moisture Content

The desorption of bound water is typically described by a kinetic equation that relates the moisture content in the cake (in percentage weight) to its equilibrium moisture content at the given temperature and pressure. The most commonly cited expression takes the form:

$$\frac{\partial c_w}{\partial t} = -k_g\left(c_w - c_w^*\right) \quad (2)$$

where c_w is moisture content (measured in % weight in the cake), k_g represents the rate constant of the desorption kinetics, and c_w^* is the equilibrium moisture content. As reported in literature,[22,33,34,38] k_g exhibits Arrhenius temperature dependence according to

$$k_g = k_{g,0}\ \exp\left(-\frac{E_a}{R_g}\left(\frac{1}{T} - \frac{1}{T^{ref}}\right)\right) \quad (3)$$

where E_a is the activation energy for water diffusion through the solid, R_g is the natural gas law constant, and $k_{g,0}$ is the rate constant at reference temperature T^{ref}. In this paper, we will use this desorption expression (Eq. 2) in our heat and mass transfer analysis for secondary drying in Section 5. We will measure the equilibrium moisture content c_w^* for sucrose and mannitol and use the cited values for the kinetic constants $k_{g,0}$ and E_a (see Table 1). We will show that precise values of c_w^*, $k_{g,0}$, and E_a will not affect heat transfer appreciably - in other words, mass transfer can be considered as one-way coupling.

Fig. 6 shows the moisture content data in the range of $-12^oC \leq T \leq 40^oC$ for 5% wt sucrose and 5% wt mannitol. For sucrose, the equilibrium moisture content appears to satisfy the relationship

$$\sqrt{c_w^*} = m_1T + m_2 \quad (4)$$

which agrees with previous data published by Kodama et al. (2014).[37] For mannitol, the moisture content exhibits two regimes. In the first regime ($T < 14.3^oC$), the equilibrium moisture content appears independent of temperature while for $T \geq 14.3^oC$ it exhibits the same scaling $\sqrt{c_w^*} = m_1T + m_2$ as sucrose.

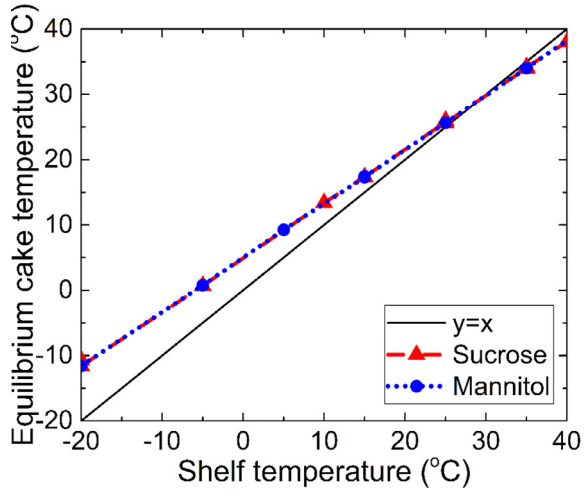

Fig. 5. Equilibrium temperature of the cake (red: sucrose, blue: mannitol) depending on the shelf temperature.

Modeling of Secondary Drying

Secondary drying is the stage of the freeze-drying cycle that immediately follows primary drying. It results from bound water desorbing from a porous cake, which is described by simultaneous heat and mass transfer equations. A schematic of the freeze-drying geometry is shown in Fig. 7. The vial is included in the domain because it contributes significantly to heat transfer.[43,46] Generally, heat is transferred to the vial from the bottom, side, or top. From the vial bottom, heat enters by conduction through direct contact with

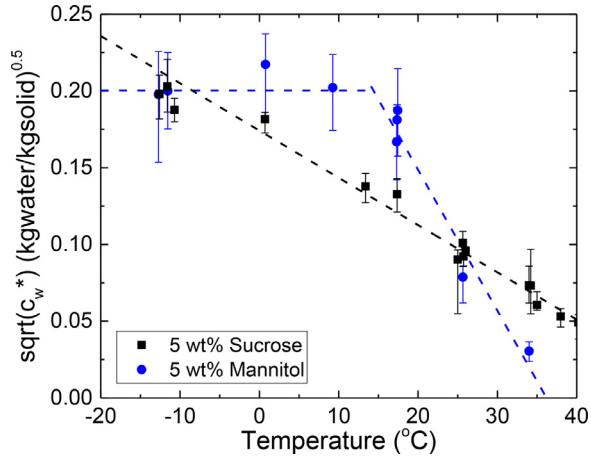

Fig. 6. Relationship between the root of equilibrium residual water content, square root of c_w^*, and the equilibrium product temperature of an aqueous solution containing 5 w/v% sugar (sucrose (rectangular) and mannitol (circle)) during secondary drying. The fit for sucrose is $\sqrt{c_w^*} = m_1T + m_2$ with m_1 = −0.00308 (kg water/kg cake)$^{0.5}$/K and m_2 = 0.17423 (kg water/kg cake)$^{0.5}$ (standard error R^2 = 0.9771). For mannitol, the fit is m_1 = 0, m_2 = 0.0401 kg water/kg cake for $T < 14.3^oC$ and m_1 = −0.00918 (kg water/kg cake)$^{0.5}$/K, m_2 = 0.33215 (kg water/kg cake)$^{0.5}$ for $T \geq 14.3^oC$ (R^2 = 0.97708).

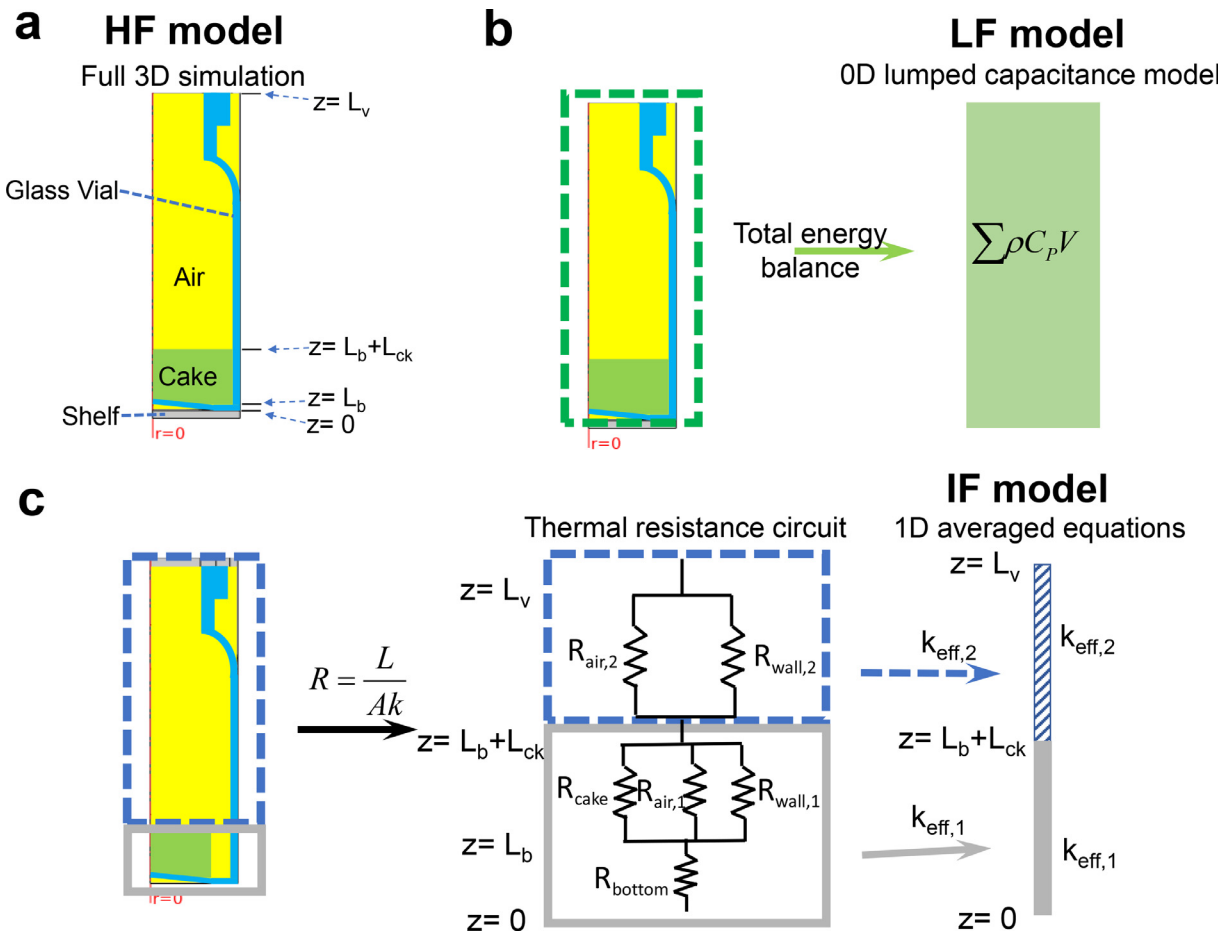

Fig. 7. System definition of each theoretical models. (a) high fidelity (HF) model, (b) low fidelity (LF) model based on 0D lumped capacitance approximation, and (c) intermediate fidelity (IF) model based on 1D averaged equations using thermal circuits.

the shelf, conduction through the gas phase between the shelf and the vial, and radiation. These effects are lumped into an effective heat transfer coefficient K_v^{sec} that was determined for secondary drying (Section 4.2). From the side, heat enters the vial either from vial-vial contacts or radiation from the chamber wall. In this study, the central vial of the shelf is completely surrounded by vials in a hexagonal array, and the aluminum blocks surrounding the vials mimic the temperature of the central vial's cake. Thus, heat transfer from the side is minimized and is expected to play a minimal role in the temperature profile. Lastly, heat transfer to the top of the vial occurs from radiation and contact with the chamber air. This again is determined by a lumped heat transfer coefficient K_{top} and will significantly affect the vial temperature if the lyophilizer has a small chamber volume (Section 4.3).

With the aforementioned boundary conditions, our secondary drying theories will consist a high fidelity model, a low fidelity model, and intermediate one with varying degrees of complexity depending on the application of interest. The high fidelity model solves the 3D temperature profile of the entire vial and the moisture content in the cake, whereas the low fidelity model examines the average temperature and moisture content in the cake via a lumped-capacitance argument. The intermediate model performs averages in the radial direction and obtains a one-dimensional equation for the temperature and moisture content. The concept of thermal circuits is used to obtain the effective thermal conductivity of system. Each model is given below.

High fidelity Model – Full 3D Simulation

We determine temperature of the cake, air, and vial by solving the full, three-dimensional energy and mass balance for the vial geometry shown in Fig. 7a. The heat and mass transfer equations are discretized by the finite element method and solved in COMSOL. Each element in the simulation is assigned different physical properties (e.g., density, heat capacity, conductivity) depending on whether the element corresponds to the cake, air, or glass. The number of elements used in the simulation is $N = 97{,}492$, and the time step is $\Delta t_s = 1$ min. We solve the following energy balance equations:

$$\rho_{ck} C_{p,ck} \frac{\partial T}{\partial t} = k_{ck} \nabla^2 T + \rho_{ck} \Delta H_v \frac{\partial c_w}{\partial t} \text{ (for cake)}, \tag{5a}$$

$$\rho_i C_{p,i} \frac{\partial T}{\partial t} = k_i \nabla^2 T \ (i = \text{other materials}) \tag{5b}$$

In the above equations, subscript i is index of the material (i = air or glass), with the quantities (ρ_i, $C_{p,i}$, k_i) being the associated density, heat capacity, and thermal conductivity. The quantities (ρ_{ck}, $C_{p,ck}$, k_{ck}) are the density, heat capacity, and thermal conductivity of the cake. The quantity T is temperature, t is time, ΔH_v is the latent heat of desorption, and c_w is moisture content at the dried cake. For Eq. (5a), the left hand side represents accumulation of energy, while the right hand side represents energy transfer from conduction and desorption. We will find from our simulations that the latent heat

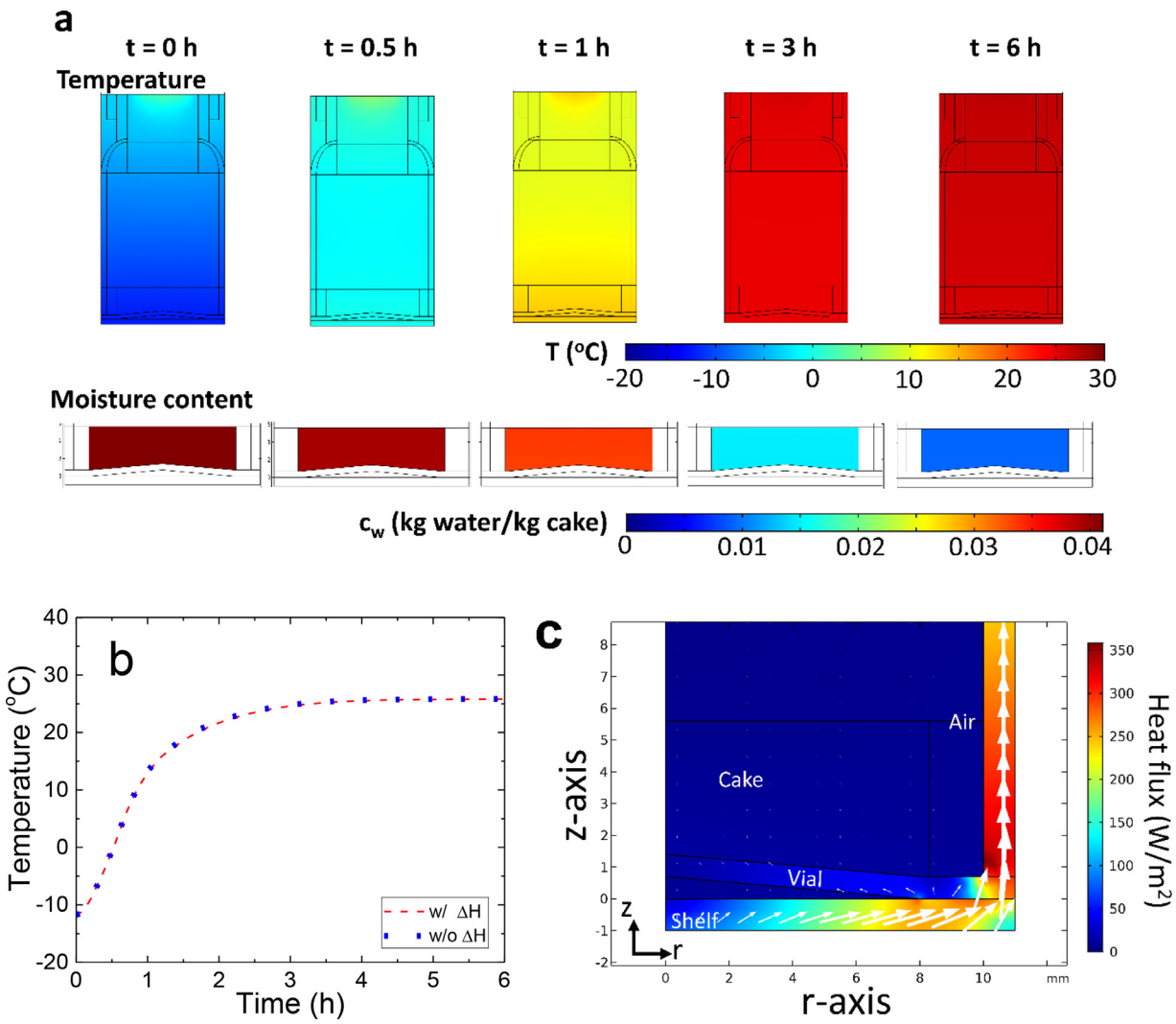

Fig. 8. (a) Temperature and moisture profile predicted from high fidelity model at different snapshots in time (0, 0.5, 1, 3, and 6 hrs into secondary drying). The initial conditions are the same experimental conditions at the end of primary drying (5 wt% sucrose cake, T = -11°C, c_w = 4.1%). (b) Comparison of the average temperature profile in the cake when one includes the enthalpy of desorption, and when one neglects this term. (c) Contour map of the heat flux with heat flux vectors at time t = 1 hr. The final shelf temperature for (a)-(c) during secondary drying is 25°C.

does not contribute much to the overall temperature profile, and thus in most situations the rightmost term in Eq. (5a) can be neglected.

At the interface between any two materials, we assume continuous temperature and continuous heat flux. The other heat transfer boundary conditions are:

$$q_{bottom} = K_v^{sec}(T_{sh} - T) \text{ at } z = 0, \tag{6a}$$

$$n \cdot \nabla T = 0 \text{ at } r = R_v, \tag{6b}$$

$$q_{top} = K_{top}(T_{top} - T) \text{ at } z = L_v \tag{6c}$$

In the above equations, q_{bottom} is the heat flux at the bottom, K_v^{sec} is heat transfer coefficient at the bottom of the vial for secondary drying, T_{sh} is the shelf temperature, T is the temperature of the material, K_{top} is the heat transfer coefficient at the top of the vial, and T_{top} is the temperature at the top of the vial. The parameters K_v^{sec}, K_{top}, and T_{top} were determined experimentally as discussed in Sections 4.2 and 4.3.

The mass transfer equation is the desorption kinetic model (Eq. 2) discussed in Section 4.4. Because the temperature profile in this model can vary spatially in the cake, the moisture content in the cake can vary spatially as well.

Fig. 8a shows typical temperature and moisture profiles predicted from this model at different snapshots in time. The initial conditions are the same experimental conditions at the end of primary drying ($T = -11^oC$, $c_w = 4.1\%$). Overall, we see that the temperature profile varies spatially in the z direction, but does not vary considerably in the r direction. Fig. 8b shows the average temperature profile in the cake when one includes the enthalpy of desorption, and when one does not include this term. The profiles are indistinguishable. These two observations suggest that one can considerably simplify our equations by considering one dimensional heat/mass transfer, and one can neglect the heat of desorption in the energy balance (thus, the mass balance can be described using one-way coupling). Lastly, Fig. 8c shows the heat flux vectors at one instant of time in the simulation (t = 1 hr into secondary drying). We see that the heat flux is predominantly routed into the glass walls, which is consistent with our order-of-magnitude analysis stating that very little heat is consumed by the cake during secondary drying (Section 4.1).

Intermediate Fidelity Model – 1D Averaged Equations

By assuming an axisymmetric geometry and dominant heat transfer only in the z-direction, one can develop an effective, 1D equation to describe the temperature profile along the vial during secondary drying. We will split our vial into two regions along the z-direction (Fig. 7c) – the region containing the cake ($0 \le z \le L_b + L_{ck}$) and the empty part of the vial ($L_b + L_{ck} \le z \le L_v$). The effective thermal conductivity of each region will be given by a thermal circuit diagram (Fig. 7c), and the total thermal mass of each region will be the sum of the thermal masses of the constitutive parts. We will also neglect the heat of desorption in the energy balance. The governing energy equations are

$$C_1 \frac{\partial T_1}{\partial t} = k_{\text{eff},1} \frac{\partial^2 T}{\partial z^2} \text{ for } 0 \le z \le L_b + L_{ck} \tag{7a}$$

$$C_2 \frac{\partial T_2}{\partial t} = k_{\text{eff},2} \frac{\partial^2 T}{\partial z^2} \text{ for } L_b + L_{ck} \le z \le L_v \tag{7b}$$

In the above equations, T_1, $k_{\text{eff},1}$ and C_1 are the temperature, effective conductivity, and thermal mass per unit volume in the first region ($0 \le z \le L_b + L_{ck}$), while T_2, $k_{\text{eff},2}$ and C_2 are the corresponding quantities in the second region ($L_b + L_{ck} \le z \le L_v$). The expressions for C_1 and C_2 are:

$$C_1 = \left(\sum_{\alpha \in \text{region } 1} \rho_\alpha C_{p,\alpha} V_\alpha \right) / \left(\sum_{\alpha \in \text{region } 1} V_\alpha \right) \tag{8a}$$

$$C_2 = \left(\sum_{\alpha \in \text{region } 2} \rho_\alpha C_{p,\alpha} V_\alpha \right) / \left(\sum_{\alpha \in \text{region } 2} V_\alpha \right) \tag{8b}$$

where α is an index for a material (cake, air, or glass), and ρ_α, $C_{p,\alpha}$, and V_α are the density, heat capacity, and volume of the material in the region of interest. The effective thermal conductivities are determined by the thermal circuit[47] in Fig. 7c. Their expressions are :

$$k_{\text{eff},1} = \frac{(L_b + L_{ck})\left(k_{ck} A_{ck} + k_{air} A_{air1} + k_{glass} A_{wall}\right) k_{glass}}{L_b \left(k_{ck} A_{ck} + k_{air} A_{air1} + k_{glass} A_{wall}\right) + k_{glass} L_{ck} A_v}, \tag{9a}$$

$$k_{\text{eff},2} = \frac{\left(k_{air} A_{air2} + k_{glass} A_{wall}\right)}{A_v} \tag{9b}$$

where k_{air} is thermal conductivity of the air, k_{ck} is thermal conductivity of the cake, k_{glass} is thermal conductivity of the glass vial, A_v is the cross-sectional area of the vial, A_{air1} is the cross-sectional area occupied by air at region 1, A_{air2} is the cross-sectional area occupied by air at region 2, A_{ck} is the cross-sectional area occupied by cake, and A_{wall} is the cross-sectional area of the glass wall (in the z-direction). The heat transfer boundary conditions for Eq. 7 are expressed as

$$-k_{\text{eff},1} \frac{\partial T_1}{\partial z} = K_v^{sec} \left(T_{sh} - T_1\right) \text{ at } z = 0 \tag{10a}$$

$$-k_{\text{eff},1} \frac{\partial T_1}{\partial z} = -k_{\text{eff},2} \frac{\partial T_2}{\partial z} \text{ at } z = L_b + L_{ck} \tag{10b}$$

$$T_1 = T_2 \text{ at } z = L_b + L_{ck} \tag{10c}$$

$$k_{\text{eff},2} \frac{\partial T_2}{\partial z} = K_{top} \left(T_{top} - T_2\right) \text{ at } z = L_v \tag{10d}$$

The mass transfer equation is the same as desorption kinetic model (Eq. 2) discussed in Section 4.4. Because of the one-way coupling nature of the equations, the desorption kinetics do not affect the temperature profile, but the temperature profile will alter the rate of desorption. We solve the temperature equations (Eq. 7) and the kinetic model (Eq. 2) with specified initial conditions using a finite difference scheme with mesh size $\Delta x_1 = (L_b + L_{ck})/5$ and $\Delta x_2 = (L_v - L_b - L_{ck})/13$ and time step $\Delta t_s = 1$ min. The initial conditions correspond to the temperature and moisture content of the vials at the end of primary drying in our experiments.

Low Fidelity Model – 0D Lumped Capacitance Model

The low fidelity model assumes uniform temperature throughout the entire vial and cake. The energy balance consists of energy accumulation in the entire vial, heat transfer from the shelf, heat transfer from the top of the vial, and enthalpy from releasing bound water:

$$\frac{dT}{dt}\left(\sum_\gamma \rho_\gamma C_{p,\gamma} V_\gamma\right) = K_v^{sec} A_v (T_{sh} - T) + K_{top} A_v \left(T_{top} - T\right) + \rho_{ck} V_{ck} \Delta H_v \frac{dc_w}{dt}; \quad 0 < z < L_v \tag{11}$$

In the above equation, $(\sum_\gamma \rho_\gamma C_{p,\gamma} V_\gamma)$ is the thermal mass of the entire vial (cake, glass, and air), A_v is the area of the bottom of the vial, ΔH_v is latent heat of desorption, and c_w is moisture content at the dried cake. This model is comparable with the empirical model that was suggested by Pisano et al. (2012) and Kodama et al. (2014).[33,37] They assumed that supplied heat was used to increase and maintain the temperature of the vial, cake, and stopper and they predicted cake temperature for secondary drying with an empirical heat capacity which was used as a fitting parameter from a preliminary run.[33,37] If one neglects the heat of desorption on the temperature profile, the above model is equivalent to a lumped capacitance model.

We note that this lumped capacitance approach should give us a qualitative picture of how temperature evolves over time, but should not be expected to be quantitative as the lumped capacitance assumption is strictly valid for Biot number $Bi \equiv \frac{K_v^{sec} L_v}{k_{\text{eff}}} < 0.1$, where k_{eff} is the effective thermal conductivity of the entire vial based on thermal circuits. In general, if one looks at freeze-drying data in the literature, the Biot number $Bi \sim O(1)$ in most setups[38,40], with the temperature distribution spatially uniform in the cake but spatially varying in the vial's air region due to the air's higher thermal resistance.

Again, the mass transfer equation is the desorption kinetic model (Eq. 2) discussed in Section 4.4. Since the temperature is spatially uniform, the energy and mass balances simplify to two ordinary differential equations for temperature and moisture content (T, c_w) in time. These differential equations are solved with specified initial conditions using a Runge-Kutta scheme in MATLAB.

Comparison Between Theory and Experiments

The three theoretical models discussed in Section 5 calculate the cake temperature and moisture content during the secondary drying process. Fig. 9 compares the temperature predictions for each of these models with experimental data for different excipients (mannitol and sucrose) and different maximum shelf temperatures ($15^oC \le T_{sh} \le 35^oC$). Since there is additional heat transfer to the top of the vial at temperature $T_{top} \approx 30^oC$ as discussed previously, the steady cake temperature at the end of secondary drying will be higher than the final shelf temperature for $T_{sh} < 30^oC$ (Fig. 9a, b, d, and e), and lower than the final shelf temperature for $T_{sh} > 30^oC$ (Fig. 9c and f).

The high fidelity model simulates the 3D temperature profile of the entire vial throughout the secondary drying process by taking account into the accurate shape of the domain such the air gap at the

bottom of the vial and geometry of the shrunken cake. Although the high fidelity model requires longer computation time than that of other models, it can be used to examine several important parameters that may be difficult to determine in the lyophilizer such as spatial and temporal distribution of the temperature, heat flux, and moisture content. It can also be used to determine hot spots in the cake which exceed the critical temperature of the cake. Overall, the high fidelity model does a good job quantitatively matching the experimental data (Fig. 9). Furthermore, if we neglect the desorption of heat in the heat balance, we get nearly identical results, indicating

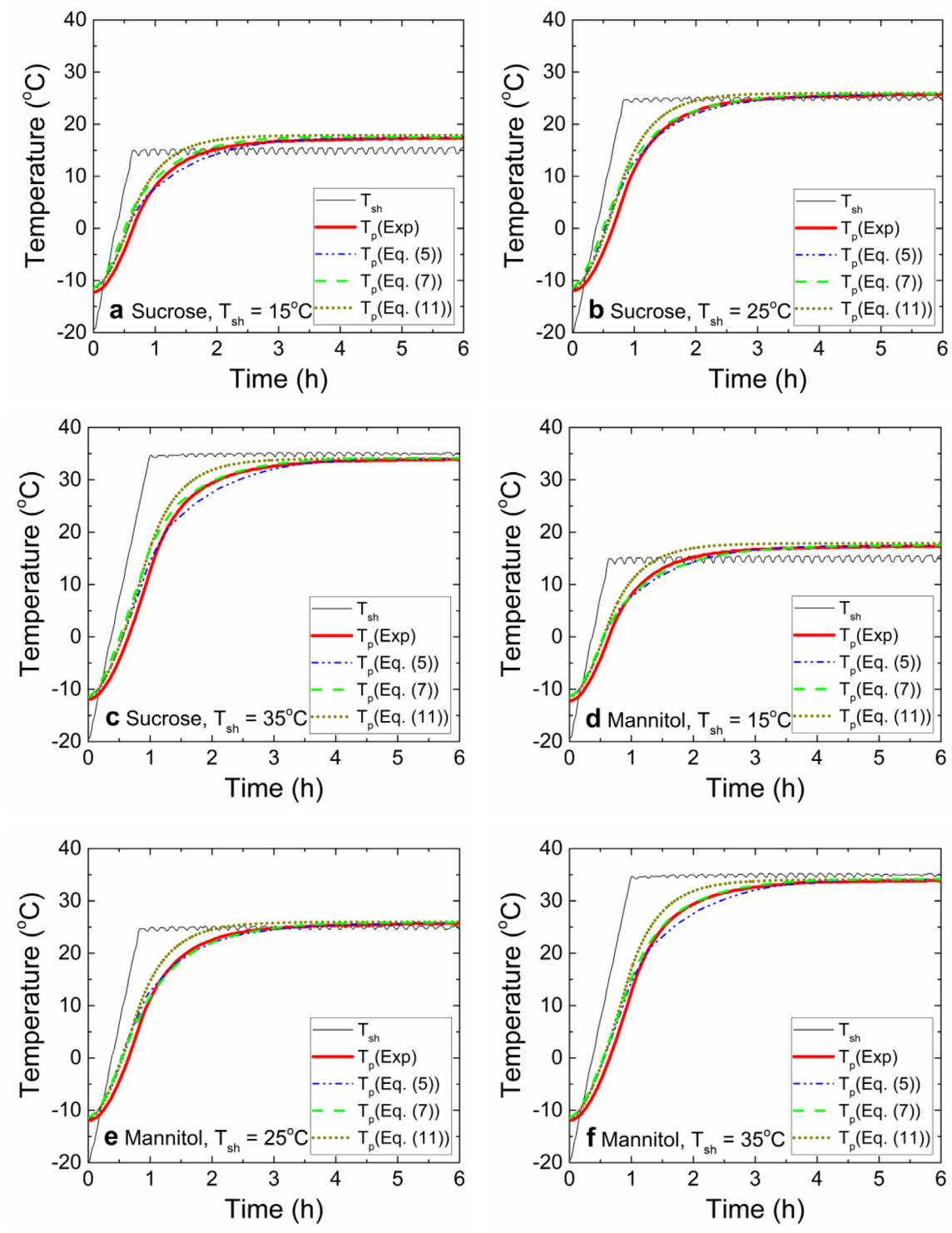

Fig. 9. Comparison of the predicted and measured product temperature profiles during secondary drying of an aqueous solution containing 5 w/v% sucrose ((a), (b), and (c)) and mannitol ((d), (e), and (f)). The shelf temperature during secondary drying process is 15°C ((a) and (d)), 25°C ((b) and (e)), and 35°C ((c) and (f)). Black: Shelf temperature, Red: Measured temperature, Blue: The predicted temperature by high fidelity model (Eq. 5), Green: The predicted temperature by intermediate fidelity model (Eq. 7), and Dark yellow: The predicted temperature by low fidelity model (Eq. 11). Note that the steady cake temperature at the end of secondary drying will be higher than setpoint for $T_{sh} = 15°C$ and $T_{sh} = 25°C$, and lower than than setpoint for $T_{sh} = 35°C$ due to the effect of the additional heat transfer at the top of the vial.

the one-way coupling of heat and mass transfer (Fig. 8b). Lastly, we show that if we artificially increase the heat capacity of the cake in our simulations by a factor of ten (Fig. S9 in Supporting Info), the temperature profile does not change appreciably, which illustrates the dominant role the vial plays in the heat transfer. If we alter the thermal properties of the vial by replacing glass with polycarbonate, we see that secondary drying is accelerated due to the polycarbonate's lower thermal mass (Fig. S10 in Supporting Info).

A low fidelity model (Eq. 11) roughly captures the experimental temperature profiles, but it tends to consistently overestimate the temperature by up to 4.5°C (Fig. 9). The reason for this overprediction comes from the fact that our system exceeds the criteria for the lumped capacitance assumption ($Bi < 0.1$). For example, an effective thermal conductivity and Biot number of the domain for 5 wt% mannitol during secondary drying process is derived as $k_{\text{eff}} = 0.301\ W/(m\ K)$ and $Bi = 0.927$, respectively, based on the thermal resistance circuit analysis. It means vertical temperature gradients are not negligible in the vial (particularly in the air region above the cake). In other words, if lumped capacitance model is applied, the temperature in the cake is overestimated while the temperature at the top of the vial is underestimated. The heat transfer at the top of the vial is also larger than the actual system.

The intermediate model solves the one dimensional temperature profile in the vial and one dimensional moisture content in the cake assuming the mass and energy balances are averaged in the radial direction. This model is considerably simpler than the full 3D simulation, yet quantitatively captures the experimental temperature data for the cake (Fig. 9). We note that it is possible to apply the intermediate model to various excipients that exhibit cake shrinkage if appropriate properties of the cake such as the thermal conductivity and cake geometry are implemented. For example, a 5wt% sucrose cake experimentally shows 17% radial direction shrinkage and 30% vertical direction shrinkage when compared to frozen solution. Our model however is able to provide accurate cake temperature for this material at different shelf temperatures as shown in Fig. 9d–f. We note because the vial dominates the heat transfer during secondary drying, one does not need exact estimates of the cake shrinkage to model the temperature profile accurately. Fig. S11 in the supporting information shows that the temperature profiles are somewhat similar if one does not take into account the cake shrinkage completely.

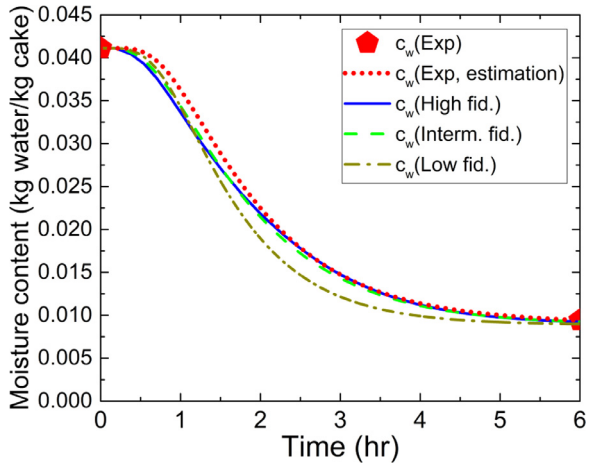

Fig. 10. The effect of temperature profile on the predicted moisture content in the cake during secondary drying of an aqueous solution containing 5 w/v% sucrose. The maximum shelf temperature during secondary drying process is $T_{sh} = 25$°C. The predicted moisture content curves are estimated from Eq. 2 with temperatures extracted from experiment (red dotted curve), high fidelity model (solid blue curve), intermediate fidelity model (dashed green curve), and low fidelity model (dash-dotted gray curve). The experimental data for the initial and final moisture content are obtained by Vapor Pro XL (Pentagon).

We lastly like to comment on the mass transfer portion of secondary drying. Because the kinetics of bound water desorption is very sensitive to temperature, the choice of heat transfer modeling will affect the moisture content in the vial considerably. For example, if one uses the low fidelity, lumped-capacitance model compared to the other two models, one will predict a lower moisture content for the same kinetic parameters (c_w^*, k_{g0}, E_a) (Fig. 10). Thus, having an appropriate heat transfer model is critical in eliminating many of the uncertainties of estimating the kinetic parameters of bound water desorption.

Conclusions

In the present study, the secondary drying stage of freeze-drying was studied experimentally by lyophilizing two different excipients (5% wt mannitol and 5% wt sucrose) under various drying conditions. For typical low fill volumes used in pharmaceutical applications (1-5 mL), we report two experimental findings:

1. The vial's thermal mass plays the dominant role in determining the temperature profile of the dried cake, with ~95% of the supplied energy used to heat the glass walls rather than the cake.
2. The vial heat transfer coefficient during secondary drying is smaller (roughly by a factor of two) than the reported values during the initial stages of primary drying, possibly due to the absence of water vapor which alters the conductivity and flowrate of the surrounding air.

There are many consequences from these observations. The first one is that secondary drying is an inherently inefficient process as very little of the supplied heat is used to desorb bound water. This observation explains why there is a strong need to develop alternative heating technologies such as microwave drying[48,49] that will specifically target the bound water rather than the vial wall. Another consequence is that the thermal properties of the cake play a small role in determining the overall temperature profile – hence why different excipients have similar temperature profiles. Lastly, up until this point, it has been assumed in the literature that the heat transfer coefficients do not change between primary and secondary drying. By performing novel experiments that measure the temperature profile and heat flux over time, we show that this assumption appears to be false. This gap in knowledge could play a key role in explaining why it appeared difficult in prior secondary drying studies to obtain quantitative agreements between experiments and theories without introducing ad-hoc fitting parameters.

In the second part of the paper, we performed heat transfer modeling and described three possible models to capture secondary drying depending on the complexity necessary for a given application – a full 3D model (high fidelity model), a 0D lumped capacitance model (low fidelity model), and a 1D averaged equation approach (intermediate model). In these models, we used the measured heat transfer coefficients for secondary drying. Overall, we see that the simplest model – the 0D lumped capacitance approach – over-predicts the cake's time-dependent temperature profile due to the fact that most vials in pharmaceutical applications have significant thermal gradients (i.e., $Bi > 0.1$). However, the full 3D simulation and 1D averaged approaches give nearly quantitative agreement with experiments with zero fitting parameters. These results seem to suggest in certain situations, secondary drying modeling can be simplified considerably by using a 1D averaged equation approach with the correct experimental heat transfer coefficients for secondary drying. In the 1D averaged approach, the energy and mass balances in the vial are averaged in the radial direction and the effective thermal conductivities are determined by a thermal

circuit analysis. Lastly, we also showed that heat of desorption does not alter the cake's temperature, and thus mass transfer can be described by one-way coupling.

Overall, we hope that this study will illuminate the essential physics related to secondary drying, and will spur innovation in developing quantitative models that can be applied to an industrial setting beyond the traditional trial-and-error approaches. We believe the intermediate model proposed here has a great potential for the precise estimation of the cake temperature along with the secondary drying time. We note that an accurate prediction of the product temperature maximizes the energy transfer and prevents overheating of the cake, which are both essential to optimization and stability. This proposed method will help find the optimal conditions for secondary drying condition under a wide range of process conditions.

Data Availability

Research data used in preparation of this manuscript is available upon request.

Declaration of Competing Interest

The authors declare that they have no known competing financial interests or personal relationships that could have appeared to influence the work reported in this paper.

Acknowledgments

The authors acknowledge the support of LyoHUB Consortium at Purdue University, and the help of Professor Alina Alexeenko, Dr. Petr Kazarin, and Dr. Andrew Strongrich from the School of Aeronautics and Astronautics. The authors declare no source of funding for this work.

Supplementary Materials

Supplementary material associated with this article can be found in the online version at doi:10.1016/j.xphs.2021.09.032.

References

1. Pikal MJ. Freeze-drying of proteins. Part I: process design. *Bio Pharm*. 1990;3(8):18–27.
2. Gatlin LA, Nail SL. Freeze drying: a practical overview. In: Harrison RG, ed. *Bioprocess Technology*. New York: Marcel Dekker, Inc.; 1993:317–367.
3. Akers MJ, Fites AL, Robinson RL. Types of parenteral administration. *J Parenter Sci Technol*. 1987;41(3):88–95.
4. Nail SL, Gatlin LA. Freeze-drying: principles and practice. In: Avis KE, Lieberman HA, Lachman L, eds. *Pharmaceutical Dosage Forms: Parenteral Medications, Vol. 2*. New York: Marcel Dekker Inc.; 1993.
5. Konstantinidis AK, Kuu W, Otten L, Nail SL, Sever RR. Controlled nucleation in freeze-drying: effects on pore size in the dried product layer, mass transfer resistance, and primary drying rate. *J Pharm Sci*. 2011;100(8):3453–3470.
6. Tang XC, Pikal MJ. Design of freeze-drying processes for pharmaceuticals: practical advice. *Pharm Res*. 2004;21(2):191–200.
7. Shivkumar G, Kazarin PS, Strongrich A, Alexeenko AA. LyoPRONTO: an open-source lyophilization process optimization tool. *AAPS PharmSciTech*. 2019;20(8):328.
8. Franks F. Freeze drying: from empiricism to predictability. *Cryo-Letters*. 1990;11(2):93–110.
9. Koganti VR, Shalaev EY, Berry MR, et al. Investigation of design space for freezedrying: use of modeling for primary drying segment of a freezedrying cycle. *AAPS PharmSciTech*. 2011;12(3):854–861.
10. Pikal MJ, Shah S, Senior D, Lang JE. Physical chemistry of freeze-drying: measurement of sublimation rates for frozen aqueous solutions by a microbalance technique. *J Pharm Sci*. 1983;72(6):635–650.
11. Kuu WY, Hardwick LM, Akers MJ. Rapid determination of dry layer mass transfer resistance for various pharmaceutical formulations during primary drying using product temperature profiles. *Int J Pharm*. 2006;313(1–2):99–113.
12. Kuu WY, Nail SL, Sacha G. Rapid determination of vial heat transfer parameters using tunable diode laser absorption spectroscopy (TDLAS) in response to step-changes in pressure set-point during freeze-drying. *J Pharm Sci*. 2009;98(3):1136–1154.
13. Kshirsagar V, Tchessalov S, Kanka F, Hiebert D, Alexeenko A. Determining maximum sublimation rate for a production lyophilizer: Computational modeling and comparison with ice slab tests. *J Pharm Sci*. 2019;108(1):382–390.
14. Roy ML, Pikal MJ. Process control in freeze drying: determination of the end point of sublimation drying by an electronic moisture sensor. *J Parenter Sci Technol*. 1989;43(2):60–66.
15. Patel SM, Doen T, Pikal MJ. Determination of end point of primary drying in freeze-drying process control. *AAPS PharmSciTech*. 2010;11(1):73–84.
16. Nail S, Tchessalov S, Shalaev E, et al. Recommended best practices for process monitoring instrumentation in pharmaceutical freeze drying—2017. *AAPS PharmSciTech*. 2017;18(7):2379–2393.
17. Pikal MJ. Use of laboratory data in freeze drying process design: heat and mass transfer coefficients and the computer simulation of freeze drying. *J Parenter Sci Technol*. 1985;39(3):115–138.
18. Liapis AI, Bruttini R. A Theory for the primary and secondary drying stages of the freeze-drying of pharmaceutical crystalline and amorphous solutes: comparison between experimental data and theory. *Sep Technol*. 1994;4(3):144–155.
19. Liapis AI, Pikal MJ, Bruttini R. Research and development needs and opportunities in freeze drying. *Dry Technol*. 1996;14(6):1265–1300.
20. Mascarenhas WJ, Akay HU, Pikal MJ. A computational model for finite element analysis of the freeze-drying process. *Comput Methods Appl Mec. Eng*. 1997;148(1–2):105–124.
21. Sadikoglu H, Liapis AI. Mathematical modelling of the primary and secondary drying stages of bulk solution. *Dry Technol*. 1997;15(3–4):791–810.
22. Pikal MJ, Cardon S, Bhugra C, et al. The nonsteady state modeling of freeze drying: in-process product temperature and moisture content mapping and pharmaceutical product quality applications. *Pharm Dev Technol*. 2005;10(1):17–32.
23. Hottot A, Peczalski R, Vessot S, Andrieu J. Freeze-drying of pharmaceutical proteins in vials: modeling of freezing and sublimation steps. *Dry Technol*. 2006;24(5):561–570.
24. Nakagawa K, Hottot A, Vessot S, Andrieu J. Modeling of freezing step during freeze-drying of drugs in vials. *AIChE J*. 2007;53(5):1362–1372.
25. Stratta L, Capozzi LC, Franzino S, Pisano R. Economic analysis of a freeze-drying cycle. *Processes*. 2020;8(11):1399.
26. Rexroad J, Wiethoff CM, Jones LS, Middaugh CR. lyophilization and the thermostability of vaccines. *Cell Preserv Technol*. 2002;1(2):91–104.
27. Pikal MJ, Shah S, Roy ML, Putman R. The secondary drying stage of freeze drying: drying kinetics as a function of temperature and chamber pressure. *Int J Pharm*. 1990;60(3):203–217.
28. Nowak D, Jakubczyk E. The Freeze-Drying of Foods—The Characteristic of the Process Course and the Effect of Its Parameters on the Physical Properties of Food Materials. *Foods*. 2020;9(10):1488.
29. Searles JA, Aravapalli S, Hodge C. Effects of chamber pressure and partial pressure of water vapor on secondary drying in lyophilization. *AAPS PharmSciTech*. 2017;18(7):2808–2813.
30. De Beer TRM, Wiggenhorn M, Veillon R, et al. Importance of using complementary process analyzers for the process monitoring, analysis, and understanding of freeze drying. *Anal. Chem*. 2009;81(18):7639–7649.
31. Fissore D, Pisano R, Barresi AA. Monitoring of the secondary drying in freeze-drying of pharmaceuticals. *J Pharm Sci*. 2011;100(2):732–742.
32. Schneid SC, Gieseler H, Kessler WJ, Luthra SA, Pikal MJ. Optimization of the secondary drying step in freeze drying using TDLAS technology. *AAPS PharmSciTech*. 2011;12(1):379–387.
33. Pisano R, Fissore D, Barresi AA. Quality by design in the secondary drying step of a freeze-drying process. *Dry Technol*. 2012;30(11–12):1307–1316.
34. Trelea IC, Fonseca F, Passot S. Dynamic modeling of the secondary drying stage of freeze drying reveals distinct desorption kinetics for bound water. *Dry Technol*. 2016;34(3):335–345.
35. Oddone I, Barresi AA, Pisano R. Influence of controlled ice nucleation on the freeze-drying of pharmaceutical products: the secondary drying step. *Int J Pharm*. 2017;524(1–2):134–140.
36. Vollrath I, Pauli V, Friess W, Freitag A, Hawe A, Winter G. Evaluation of heat flux measurement as a new process analytical technology monitoring tool in freeze drying. *J Pharm Sci*. 2017;106(5):1249–1257.
37. Kodama T, Takeuchi M, Wakiyama N, Terada K. Optimization of secondary drying condition for desired residual water content in a lyophilized product using a novel simulation program for pharmaceutical lyophilization. *Int J Pharm*. 2014;469(1):59–66.
38. Sahni EK, Pikal MJ. Modeling the secondary drying stage of freeze drying: development and validation of an excel-based model. *J Pharm Sci*. 2017;106(3):779–791.
39. Assegehegn G, Brito-de la Fuente E, Franco JM, Gallegos C. Understanding and optimization of the secondary drying step of a freeze-drying process: a case study. *Dry Technol*. 2021;39(8):1003–1017.
40. Ravnik J, Golobič I, Sitar A, et al. Lyophilization model of mannitol water solution in a laboratory scale lyophilizer. *J Drug Deliv Sci Technol*. 2018;45:28–38.

41. Moino C, Bourlés E, Pisano R, Scutellà B. In-line monitoring of the freeze-drying process by means of heat flux sensors. *Ind Eng Chem Res*. 2021;60(26):9637–9645.
42. Joseph E. Residual moisture determination in lyophilized drug products. *Pharm Technol*. 2019;43(11):30–39. 56.
43. Brülls M, Rasmuson A. Heat transfer in vial lyophilization. *Int J Pharm*. 2002;246(1–2):1–16.
44. Rambhatla S, Obert JP, Luthra S, Bhugra C, Pikal MJ. Cake shrinkage during freeze drying: a combined experimental and theoretical study. *Pharm Dev Technol*. 2005;10(1):33–40.
45. Ullrich S, Seyferth S, Lee G. Measurement of shrinkage and cracking in lyophilized amorphous cakes. Part II: kinetics. *Pharm Res*. 2015;32(8):2503–2515.
46. Pikal MJ, Roy ML, Shah S. Mass and heat transfer in vial freeze-drying of pharmaceuticals: role of the vial. *J Pharm Sci*. 1984;73(9):1224–1237.
47. Swift G, Molinski TS, Lehn W. A fundamental approach to transformer thermal modeling—part I: theory and equivalent circuit. *IEEE Trans Power Del*. 2001;16(2):171–175.
48. Feng H, Yin Y, Tang J. Microwave Drying of Food and Agricultural Materials: Basics and Heat and Mass Transfer Modeling. *Food Eng Rev*. 2015;4(2):89–106.
49. Gitter JH, Geidobler R, Presser I, Winter G. Significant drying time reduction using microwave-assisted freeze-drying for a monoclonal antibody. *J Pharm Sci*. 2018;107(10):2538–2543.